www.sciencemag.org/content/357/6355/1037/suppl/DC1

Supplementary Materials for

Sterilizing immunity in the lung relies on targeting fungal apoptosis-like programmed cell death

Neta Shlezinger, Henriette Irmer, Sourabh Dhingra, Sarah R. Beattie, Robert A. Cramer, Gerhard H. Braus, Amir Sharon,* Tobias M. Hohl*

*Corresponding author. Email: hohlt@mskcc.org (T.M.H.); amirsh@tauex.tau.ac.il (A.S.)

Published 8 September 2017, *Science* **357**, 1037 (2017)
DOI: 10.1126/aan0365

This PDF file includes:

Materials and Methods

Reagents and Antibodies

Chemical and cell culture reagents were purchased from Thermo Scientific and Gibco, unless noted otherwise. Voriconazole (Pfizer) was obtained from the Memorial Sloan Kettering Cancer Center pharmacy and dissolved in sterile PBS at 10 mg/ml and stored at -80^{o}C. Fluorescent antibodies were from Tonbo or eBioscience. S12 *SURVIVIN* antagonist was purchased from Calbiochem (#574661).

Mice, Animal Care, and Ethics Statement

C57BL/6 (Jackson Laboratories, strain 000664; CD45.2^{+}), C57BL/6.SJL (Charles River Laboratories, strain 564; CD45.1^{+}), and p91phox$^{-/-}$ mice (Jackson Laboratories, strain 002365) were bred in the MSKCC Animal Vivarium. p91phox$^{-/-}$ mice were crossed to the C57BL/6.SJL background. Lethally irradiated (9.5 Gy) F1 progeny (from cross of C57BL/6 and C57BL/6.SJL strains) were reconstituted with 1-2.5 x 10^{6} CD45.2^{+} C57BL/6 and with 1-2.5 x 10^{6} CD45.1^{+} p91phox$^{-/-}$ bone marrow cells, treated with enrofloxacin in the drinking water for 21 days to prevent bacterial infections, and rested for 6-8 weeks prior to use. All animal experiments were conducted with sex- and age-matched mice and performed with approval from MSKCC Institutional Animal Care and Use Committee (protocol number 13-07-008). Animal studies complied with all applicable provisions established by the Animal Welfare Act and the Public Health Services Policy on the Humane Care and Use of Laboratory Animals.

Fungal growth and culture

All *A. fumigatus* strains were grown on glucose minimal media that contains 1% glucose, salt solution, and trace minerals, or on Sabouraud medium, at 37°C (*22*). Conidia were harvested by flooding 5-10 day old plates or slants with 10 ml PBS, 0.025% Tween-20, briefly agitating sealed plates or slants on a vortex shaker, and by filtering the conidial suspensions twice through a 40 μm nylon cell strainer. For RNA analysis, 10^5 conidia/ml were grown in RP-10^+ (i.e., RPMI 1640, 10% heat-inactivated fetal bovine serum (FBS), 5 mmol/L HEPES [pH 7.4], 1.1 mmol/L L-glutamine, 0.5 U/ml penicillin, 0.5 μg/ml gentamicin, 50 mg/ml streptomycin, and 50 mol/l 2-mercaptoethanol) in baffled flasks at 37°C under agitation (200 RPM) for 20 h. 10^6 conidia/ml were incubated in RP-10^+ for 8 h at 37°C to prepare germlings, or in RP-10^+ supplemented with 0.5 μg/ml voriconazole for 14 h at 37°C to generate uniform preparations of swollen conidia, as described in (*23*). Resting conidia were labeled with Alexa Fluor 633 as described in (*10*).

Generation of *H-RFP* and *BIR1* transgenic strains

To generate the *H-RFP* strain, *A. fumigatus* ATCC 46645 was transformed with pME3857 (*24*) and transformants were selected with 30 μg/ml phleomycin (*25*) (Table S1). In the *H-RFP* strain, nuclei are tagged with a histone 2A-mRFP fusion protein.

The *A. fumigatus* Af293 genome sequence (http://www.broad.mit.edu) was used to design primers for the amplification of the *AfBIR1* gene (Table S2). *A. fumigatus* genomic DNA was isolated as described in (*26*). The full-length *AfBIR1* gene (1-2820 bp) was amplified from genomic DNA with Phusion polymerase and primers 1 and 2. The resulting amplification product was sequenced and cloned into the Pme I site (downstream to the *A. nidulans* GpdA promoter and upstream to its terminator) of pSK379 to produce the overexpression vector

PskBIR1. The *H-RFP* and the ATCC 46645 strains were transformed with PskBIR1 and transformants selected on 2 µg/ml pyrithiamine.

For overexpression of the N terminal part of the protein, nucleotides 0-1545 bp of *AfBIR1* containing both BIR domains, were amplified with primers 1/3 and cloned into the PmeI site in pSK379 to produce the N-BIR1 overexpression cassette. To generate the $bir1_{\text{tetON}}$ strain, a 1.6kb fragment upstream of the *BIR1* promoter was amplified with primers 12 and 13 (with an AscI restriction site) and a 1.3kb bir1 genomic fragment was amplified with primers 14 (with a PacI restriction site) and 15. The two PCR products were fused together using fusion PCR (*31*) with nested primers 16 and 17, generating AscI and PacI restriction sites between the two PCR fragments. The resulting 2.7kb fragment was ligated into the pJET1.2 cloning vector (Thermo Fisher Scientific, USA) as per manufacturer's guidelines generating plasmid pBir1. The tetON module was amplified with primers 18 (with AscI restriction site) and 19 (with PacI restriction site) from pSK541_pJW121 (a kind gift from Dr. Sven Krappmann) (*32*). The tetON module was digested with AscI and PacI and ligated into pBir1 generating pBir2. The *H-RFP* strain was transformed using a split marker approach (*33*), using primers 16/20 and 17/21 to amplify P1 and P2 from pBir1. The transformants were selected on plates containing 0.1µg/ml pyrithiamine hydrobromide and 0.5 µg/ml doxycycline hyclate (Sigma, USA).

Radial growth, conidiation, and germination assays

Radial growth on solid media was obtained by measuring colony diameters every 24 h over a period of 7 d starting with an inoculum of 10^3 conidia on Sabouraud agar grown at 37°C. Conidiation was quantified by harvesting from 4 d old Sabouraud agar plates that were inoculated with 10^3 conidia per plate. The conidial concentration was determined by counting

with a hemocytometer. To determine the germination rate, conidia (1×10^6 conidia/ml) from each strain were inoculated into RP-10^+ and incubated at 37°C for 24 h. Conidial samples were removed at 4, 6, 8, 10, 12, 16, and 24 h and germination rates were determined by scoring 100 conidia for germination.

PCD assays and staining procedures

A-PCD was determined by analyzing the following markers: loss of histone 2A RFP fluorescence, detection of fungal caspase activity, and accumulation of DNA-strand breaks by TUNEL (*19, 27*). Fungal cell viability was determined by plating and measurement of colony forming units (CFUs). DNA double-strand breaks were detected by TUNEL using the *APO-BrdU™ TUNEL Assay Kit* (Molecular Probes™, A23210), as previously described (*28*). Briefly, fungal cells were fixed with 3.7% formaldehyde, digested with lysing enzyme (Sigma Corp., L1412), rinsed with PBS, incubated in ice-cold 70% (v/v) ethanol, washed with washing buffer, incubated with 50 µl TUNEL labeling mixture at 37^{o}C for 70 min with agitation and rinsed 3 times with rinse buffer and incubated in 100 µL of antibody staining solution (Alexa Fluor® 488 labeled anti-BrdU antibody) for 30 min. The CaspACE in situ marker fluorometric assay system that utilizes the FITC-VAD-fmk probe (Promega Corp., G7461) was used to stain for fungal caspase activity.

Briefly, fungal cells were harvested, washed in PBS, and resuspended in 50µl of staining solution containing 10 µM FITC-VAD-fmk. After incubation for 20 min at RT with low agitation in darkness, cells were washed twice with PBS and analyzed by fluorescence microscopy or flow cytometry. For sorted neutrophils that contained ingested conidia,

phagocytes were first lysed osmotically by incubation in distilled water prior to staining with FITC-VAD-fmk or by TUNEL.

Microscopy

Epifluorescence and light microscopy were performed with a Zeiss Axio imager M1 microscope. Differential interference microscopy (DIC) was used for bright field images. Images of TUNEL staining in Fig. S1 were acquired with a Zeiss LSM880 confocal microscope. The following filters were used for examination of fluorescent samples: DAPI filter (excitation 340–390 nm, emission 420–470 nm), rhodamine filter (excitation 540–552 nm, emission 575–640 nm), GFP filter (excitation 450–490 nm, emission 500–550 nm). Images were captured with a Zeiss AxioCam MRm camera and analyzed using Axiovision Rel 4.5 software package. Image processing was performed using ImageJ 1.42q software (http//rsb.info.nih.gov/ij/).

Analysis of infected mice

Mice were infected via the intratracheal route as described in (*29*). BAL and lung suspensions were prepared for flow cytometry as described in (*16*). Briefly, lung digest and, if applicable, BAL cells were enumerated and stained with the following Abs: anti-Ly6C (clone AL-21), anti-Ly6G (clone 1A8), anti-CD11b (clone M1/70), anti-CD11c (clone HL3), anti-CD45.1 (clone A20), anti-CD45.2 (clone 104), anti-Ly6B.2 (clone 7/4), anti-MHC class II (clone M5/114.15.2), anti-Siglec F (clone E50-2440) and CD103 (clone 2E7). Neutrophils were identified as $CD45^{+}CD11b^{+}Ly6C^{lo}Ly6G^{+}$ cells, inflammatory monocytes as $CD45^{+}CD11b^{+}Ly6C^{hi}Ly6G^{-}Ly6B.2^{+}$ cells, Mo-DCs as $CD45^{+}CD11c^{+}$MHC class II^{+} $CD11b^{+}CD103^{-}SiglecF^{-}$ cells, and alveolar macrophages as

$SSC^{hi}CD45^{+}CD11b^{+}CD11c^{+}$ $SiglecF^{+}$ bronchoalveolar lavage fluid cells. Flow cytometry data was collected on a BD LSR II flow cytometer and analyzed on FlowJo, version 9.7.6 (Treestar). Perfused murine lungs were homogenized in 2 mL of PBS, 0.025% Tween-20 for colony-forming units (CFUs) and for ELISA. For histology, perfused lungs were fixed in 10% neutral-buffered formalin, embedded in paraffin, sectioned in 4 μm slices, and stained with hematoxylin & eosin (H&E), Gomori's ammoniacal silver (GAS) or Uvitex 2B. Slides were reviewed by a board-certified pathologist and evaluated in a blinded manner. Whole section images were digitally scanned using the Zeiss Mirax Desk Scanner for high-resolution viewing and automated cell counting. Images were captured from whole slide images, acquired with the Aperio ScanScope (Aperio Technologies) using ×20 and ×40 objectives.

Statistical analysis.

Data are presented as a mean ± SEM or ±SD for each group and derived from experiments performed in triplicate, unless stated otherwise. For 3 or more groups, statistical significance was determined by Kruskal-Wallis one-way analysis of variance followed by Dunn's post-test. The Mann-Whitney U test was used for two non-parametric groups of data. Survival data was analyzed by log rank test. All statistical analyses were performed with GraphPad Prism software, v6.0c.

Supplementary Figures:

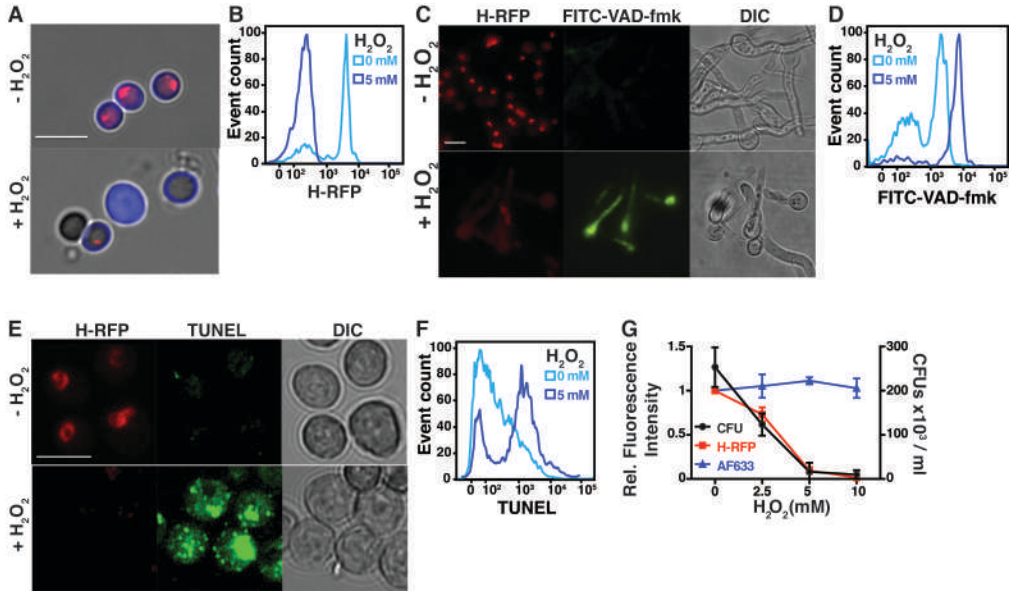

Figure S1. Apoptosis-like PCD in *A. fumigatus.*

(A) Fluorescence microscopy and (B) flow cytometric analysis of *H-RFP* conidia after 6 h exposure to 0 mM (upper panel) or 5 mM H_2O_2 (lower panel). Scale bar = 10 µm. (A) Conidia were conjugated to AF633 (blue fluorescence signal) and fluorescence images were overlaid on differential interference contrast (DIC) images. (C) Fluorescence and DIC microscopy and (D) flow cytometric analysis of *H-RFP* germlings stained with FITC-VAD-fmk after 4 h exposure to 0 mM (upper panel) or 5 mM H_2O_2 (lower panel). Scale bar = 10 µm. (E) Confocal microscopy and (F) flow cytometric analysis of *H-RFP* conidia stained by TUNEL after 6 h exposure to 0 mM (upper panel) or 5 mM H_2O_2 (lower panel). Scale bar = 5 µm. (G) Relative RFP (red squares) and AF633 (blue triangles) fluorescence intensities and fungal CFUs (black circles) for AF633-labeled *H-RFP* conidia after 6 h exposure to 0-10 mM H_2O_2. The fluorescence intensities are indicated relative to conidia not treated with H_2O_2. Data are indicated as mean ± standard deviation from triplicate samples of a representative experiment.

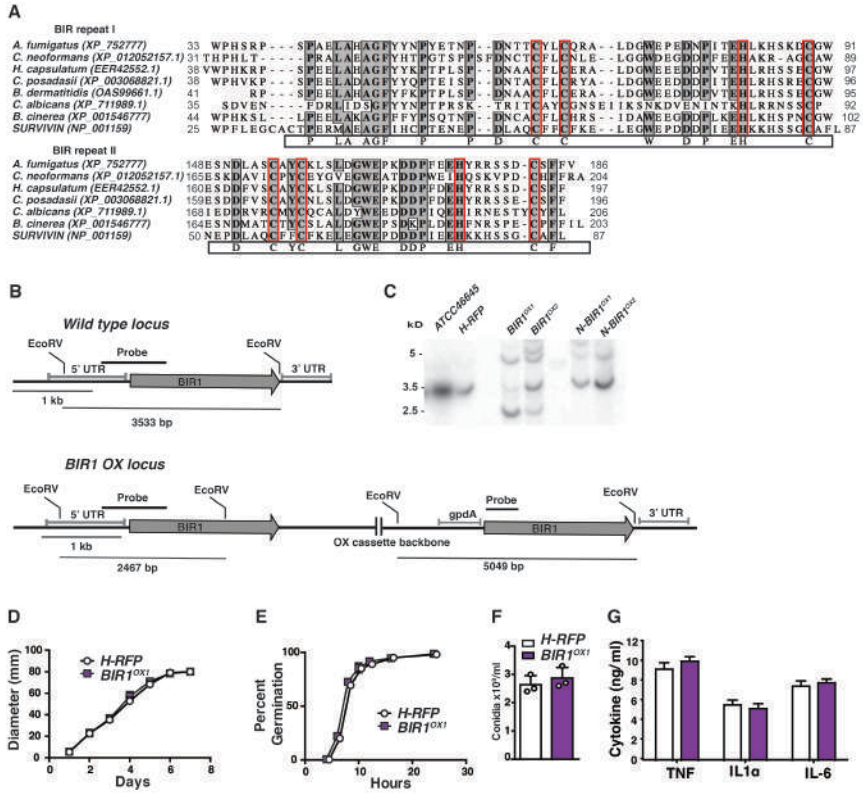

Figure S2. *AfBIR1* is a human SURVIVIN homolog.

(A) Alignment of the amino acid sequence of the first (upper panel) and second (lower panel) BIR repeats in *Aspergillus fumigatus BIR1* with the first and second BIR domains in the *Cryptococcus neoformans*, *Histoplasma capsulatum*, *Coccidioides posadasii*, *Blastomyces dermatitidis*, *Candida albicans, and Botrytis cinerea* homologues, respectively. The single BIR domain of the human *SURVIVIN* gene is included in both comparisons. The alignment was generated using ClustalW. The consensus sequence and conserved C2HC residues are marked by black and red squares, respectively.

(B) Graphical representation of the predicted *BIR1* genomic locus in wild-type and in *BIR1*^{OX} strains. The grey arrows indicate the orientation of the *BIR1* gene. In *BIR1* overexpression strains, the circular expression vector is integrated into the endogenous *BIR1* locus, resulting in

two *BIR1* copies: the genomic copy under control of the gpdA promoter and the plasmid cDNA copy under control of the endogenous promoter. An 860 bp fragment (black line, probe) was used for Southern blot analysis.

(C) Southern blot analysis of full-length and N-terminal (1-1545 bp) domain $BIR1^{OX}$ strains. The expected band size was 3.5 kb in the parental *H-RFP* and *ATCC 46645* strains, reflecting the presence of a wild-type *BIR1* locus. In the $BIR1^{OX}$ strains, two additional bands were expected, with a size of 5.0 kb and 2.5 kb. In the $N\text{-}BIR1^{OX}$ strains, an EcoRV restriction site is lost, resulting in the additional 5.0 kb band and loss of the additional 2.5 kb band.

(D-G) Characterization of the $BIR1^{OX1}$ strain. The plots show (D) radial growth over a 7-day time course, (E) conidial germination over a 24 h time course, and (F) conidiation rates for *H-RFP* (white circles and bars) and BIR^{OX1} conidia (purple squares and bars). (E) The percent germination is based on analysis of 100 conidia under light microscopy (magnification, ×400), repeated in triplicate, for each sample. (G) The bar graphs show the mean + SD cytokine responses by cultured macrophage (MH-S cells) following 24 h co-incubation with irradiated *H-RFP* or $BIR1^{OX1}$ swollen conidia.

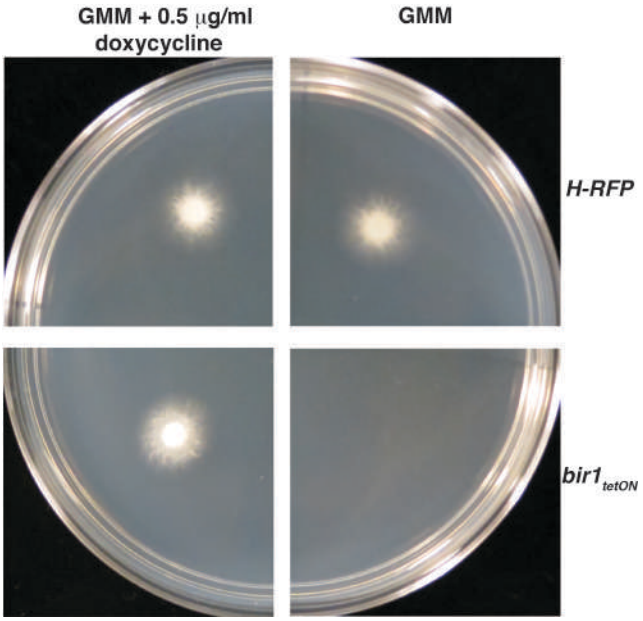

Figure S3. BIR1 is an essential gene.

Doxycycline dependent growth of the *bir1*$_{\text{tetON}}$ strain. One thousand *H-RFP* (top row) or *bir1*$_{\text{tetON}}$ (bottom row) conidia were point inoculated on GMM plates supplemented with 0.5 μg/ml doxycycline (left column) or not (right column). Plates were incubated at 37˚C for 36 hours and photographed.

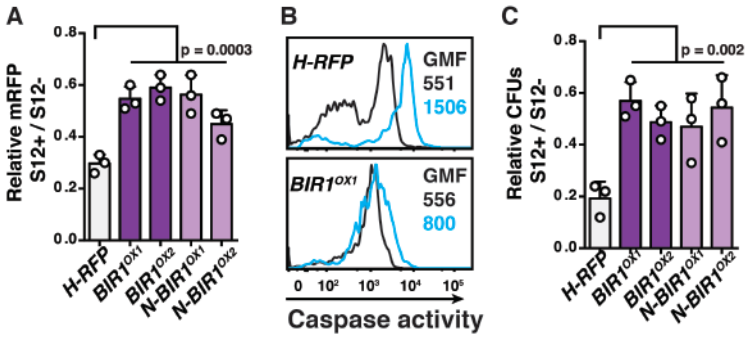

Figure S4. The *SURVIVIN* antagonist S12 induces A-PCD in *A. fumigatus*.

The plots show (A) relative mRFP fluorescence, (B) fungal caspase activity, and (C) relative CFUs in the indicated strains (*H-RFP*, white bars; $BIR1^{OX1,2}$, dark purple bars; $N\text{-}BIR1^{OX1,2}$, light purple bars in A and C) following exposure to 200 µM S12 (S12+) or not (S12-). The experiments were performed with (A, C) swollen conidia or (B) germlings that were exposed to S12 (light blue line in panel B) or not (black line in panel B) for (A, C) 8 h or (B) 4 h. GMF, geometric mean fluorescence. Data are represented as the relative mean + standard deviation of 3 independent experiments performed with triplicate samples that were pooled and represented as a circle. Statistical analysis: One-way analysis of variance (ANOVA) followed by Dunnett's multiple comparisons.

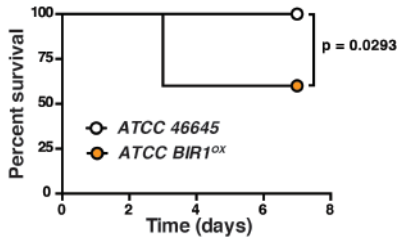

Figure S5. Murine survival following challenge with a *BIR1*^{OX} strain that lacks the *H-RFP* transgene. Survival of C57BL/6 mice challenged with 6 x 10^7 *ATCC 46645* (white circles) or *ATCC BIR1*^{OX} (orange circles) conidia (n = 10 per group). Statistical analysis: Log-rank (Mantel-Cox) test.

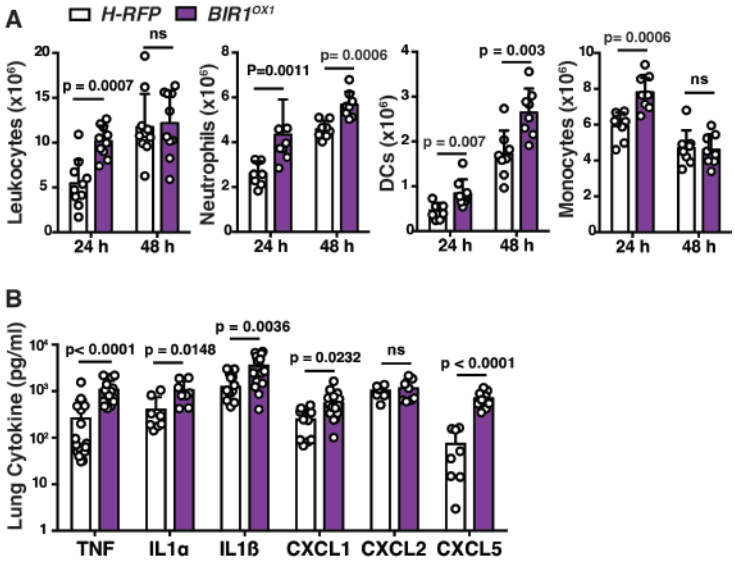

Figure S6. Pulmonary leukocyte recruitment and cytokine levels in *BIR1*^{OX1} and *H-RFP*-challenged mice. C57BL/6 mice challenged with 3 x 10^7 *H-RFP* (white bars) and *BIR1*^{OX1} (dark purple bars) conidia and analysed for (A) lung leukocytes and (B) lung cytokine levels at 24 hpi. (A, B) Data were pooled from two independent experiments, with individual mice denoted as circles, and represented as the mean + standard deviation. Statistical analysis: Mann Whitney test.

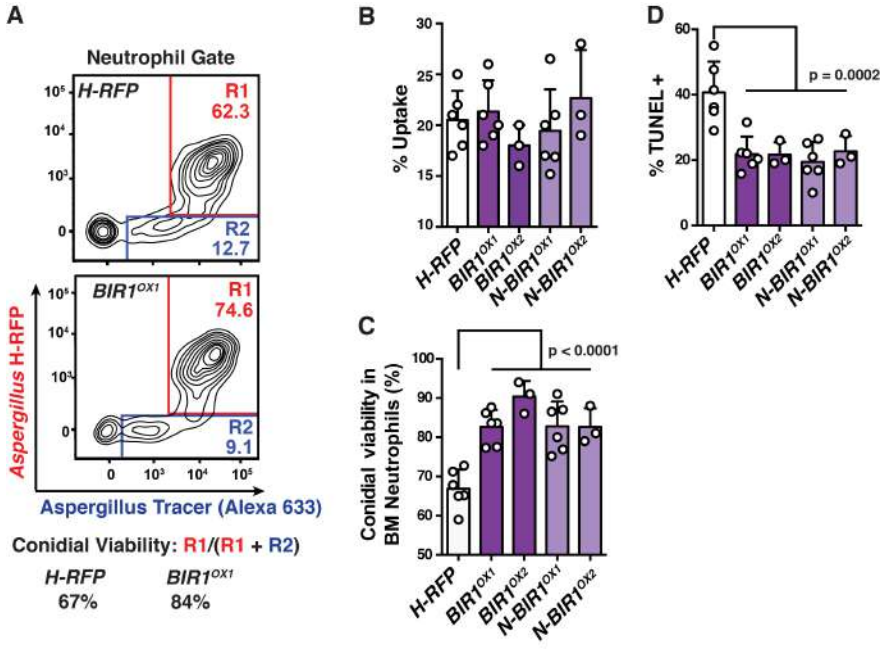

Figure S7. Murine neutrophils differentially induce of apoptosis-like PCD in conidia on the basis of *BIR1* expression levels.

Murine bone marrow neutrophils were analyzed on the basis of conidial RFP and Alexa 633 fluorescence (MOI = 3, 8 h co-incubation at 37^{o}C). (A) Representative plots. For the indicated fungal strains, Gate R1 (red) indicates neutrophils that contain live conidia, and gate R2 neutrophils that contain killed conidia. The bar graphs show the average frequency of (B) conidial uptake (R1 + R2) by neutrophils and (C) of live conidia [R1/(R1+R2)] in fungus-engaged neutrophils. (D) The average frequency of TUNEL^{+} nuclei for each fungal strain. Error bars represent mean + standard deviation of 3-6 independent experiments performed in triplicates. Statistical analysis: One-way analysis of variance (ANOVA) followed by Dunnett's multiple comparisons test.

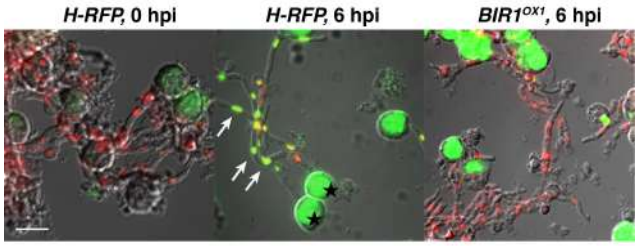

Figure S8. Human neutrophils differentially induce of A-PCD in fungal conidia and hyphae on the basis of *BIR1* expression levels.

Germlings were co-incubated with human neutrophils (MOI = 3, 6 h). Fluorescence microscopy of *H-RFP* and *BIR1*^{OX1} hyphae stained for DNA fragmentation by TUNEL. TUNEL^{-} hyphal nuclei appear red due to the *H-RFP* transgene (left and right panels), while TUNEL^{+} nuclei appear green (white arrows, middle panel). The green staining in large circular cells (black stars) represents neutrophil DNA fragmentation. Scale bar = 10 μm.

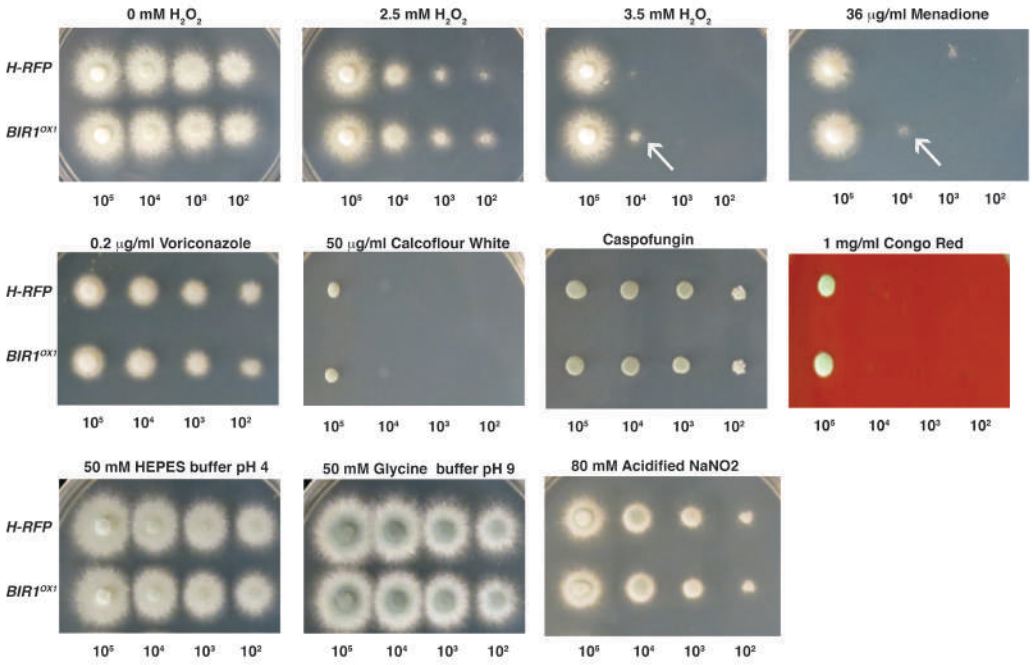

Figure S9. BIR1 overexpression is protective against oxidative stress.

H-RFP and *BIR1*^{OX1} conidia were adjusted to 10^5, 10^4, 10^3, and 10^2 in 2 µl H_2O and point inoculated on GMM plates with the indicated stress. Plates were incubated at 37^{o}C (5% CO_2) for 48 h and photographed. H_2O_2 and menadione represent oxidative stress; voriconazole, Calcofluor White, caspofungin, and Congo Red represent various agents of cell wall stress; $NaNO_2$ represents nitrogenous stress.

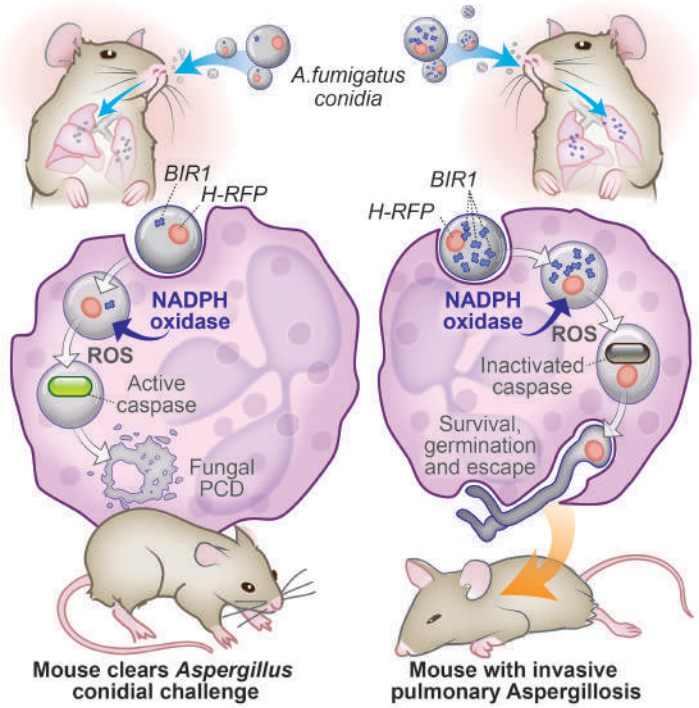

Figure S10. A model showing the role of fungal PCD in early events of *A. fumigatus* infection. Following *A. fumigatus* inhalation, innate phagocytic cells are recruited to the lungs and airways and ingest conidia. NADPH oxidase is assembled on the phagosomal membrane to generate ROS, which trigger caspase activity and A-PCD in swollen conidia. An anti-apoptotic machinery, mediated by *AfBIR1*, resists NADPH oxidase-mediated killing by inhibiting fungal caspase activity and surviving conidia manage to germinate and escape the phagolysosomal environment, resulting in invasive aspergillosis.

Table S1. List of Strains and Plasmids

Strain or Plasmid	Genotype and Description	Source
Aspergillus fumigatus		
ATCC 46645	*A. fumigatus* wt strain	ATCC
H-RFP	Histone H2A:: mRFP gene fusion	This work
BIR1^{OX}	Overexpression of full-length *AfBIR1* (amino acids 1-871)	This work
N-BIR1^{OX}	Overexpression of N terminal *AfBIR1* domain (amino acids 1-446)	This work
Plasmids		
pME3857	gpdA::mrfp::h2A::trpCt (histone 2A) with phleomycin resistance marker	(*24*)
pSK379	Plasmid contains ^{p}gpdA::his2a^{t}::ptrA	(*30*)
pSKBIR1	Full-length *AfBIR1* overexpression	This work
pJET1.2	cloning vector	Thermo Fisher Scientific, USA
pSK541_pJW121	ptrA; gpdA::rtTA::TcgrA, tetO7::pmingpdA (tet module)	(*32*)

pBir1	Upstream region of *AfBIR1* and 1.3kb of *AfBIR1* in the cloning site of pJET1.2	This work
pBir2	tet module from pSK541_pJW121 in between *AfBIR1* upstream region and *AfBIR1* genomic sequence in pBir1	This work

Table S2. List of Oligonucleotides.

	Oligonucleotide	**Sequence (5' to 3')**
1	BIR1-FOR-PmeI	AGT TTA AAC ATG GAG ACT TTC GCC G
2	BIR1-REV-PmeI	TGT TTA AAC TCA ATC AAT GCA CTC G
3	N-BIR1-REV- PmeI	TGT TTA AAC TTA GTC GAC AGT ATC GTG CTG CAC CTT GGG T
4	BIR1-RT-FOR	CCT CGC CAG CTT TGA TCT G
5	BIR1-RT-REV	GGA TTG GTC TCG TAG GGA TTG
6	βtubulin-RT-FOR	GGC TTT CTT GCA TTG GTA CAC
7	βtubulin-RT-REV	AGA TCG TTC ATG TTG CTC TCG
8	GpdH-RT-FOR	TTG AAG ATT CCC GAA GCC TAC
9	GpdH-RT-REV	TCG TCA AGG TAG TGT AGG AGA G
10	BIR1-SOUTHERN-FOR	ATT TCC ATT ACA GCC GAA CG
11	BIR1-SOUTHERN-REV	ATT GAG AAC ATG TCG AAC AC
12	RAC4114	CCC TAC AGA CTG CTA TCA TCC TGC
13	RAC4115	ACC GGT CGC CTC AAA CAA TGC TCT GGC GCG CCG TAG TTA TCT CTG CAA GCT GCT CG
14	RAC4116	AGA GCA TTG TTT GAG GCG ACC GGT TAA TTA ATG GAG ACT TTC GCC GCC
15	RAC4117	CGG TAA CCG AGC TTC CAG AGC
16	RAC4118	CGT CAG ACT TAG GCC GCT ATG TAC G
17	RAC4119	GTC GGA GGT TCG GAT TGG TG
18	RAC2412	AAA AAA AAG GCG CGC CGA GCT CGA GGT CGA CGG TAT CGA T

19	RAC2413	AAA AAA AAT TAA TTA AGT TTA AAC GGT GAT GTC TGC TCA AGC G
20	RAC4181	GCG GTC TGA GCA CTG CGT AC
21	RAC4182	GTC CAG TTG ACG ACA ACA CCA GC

References

1. S. Nagata, M. Tanaka, Programmed cell death and the immune system. *Nat*. *Rev*. *Immunol*. **17**, 333–340 (2017). doi:10.1038/nri.2016.153 Medline

2. I. Jorgensen, M. Rayamajhi, E. A. Miao, Programmed cell death as a defence against infection. *Nat*. *Rev*. *Immunol*. **17**, 151–164 (2017). doi:10.1038/nri.2016.147 Medline

3. G. D. Brown, D. W. Denning, N. A. Gow, S. M. Levitz, M. G. Netea, T. C. White, Hidden killers: Human fungal infections. *Sci*. *Transl*. *Med*. **4**, 165rv13 (2012). doi:10.1126/scitranslmed.3004404 Medline

4. S. L. Gerson, G. H. Talbot, S. Hurwitz, B. L. Strom, E. J. Lusk, P. A. Cassileth, Prolonged granulocytopenia: The major risk factor for invasive pulmonary aspergillosis in patients with acute leukemia. *Ann*. *Intern*. *Med*. **100**, 345–351 (1984). doi:10.7326/0003-4819-100-3-345 Medline

5. B. H. Segal, Aspergillosis. *N*. *Engl*. *J*. *Med*. **360**, 1870–1884 (2009). doi:10.1056/NEJMra0808853 Medline

6. V. Espinosa, A. Jhingran, O. Dutta, S. Kasahara, R. Donnelly, P. Du, J. Rosenfeld, I. Leiner, C. C. Chen, Y. Ron, T. M. Hohl, A. Rivera, Inflammatory monocytes orchestrate innate antifungal immunity in the lung. *PLOS Pathog*. **10**, e1003940 (2014). doi:10.1371/journal.ppat.1003940 Medline

7. C. Veneault-Fourrey, M. Barooah, M. Egan, G. Wakley, N. J. Talbot, Autophagic fungal cell death is necessary for infection by the rice blast fungus. *Science* **312**, 580–583 (2006). doi:10.1126/science.1124550 Medline

8. N. Shlezinger, A. Minz, Y. Gur, I. Hatam, Y. F. Dagdas, N. J. Talbot, A. Sharon, Anti-apoptotic machinery protects the necrotrophic fungus *Botrytis cinerea* from host-induced apoptotic-like cell death during plant infection. *PLOS Pathog*. **7**, e1002185 (2011). doi:10.1371/journal.ppat.1002185 Medline

9. A. Konishi, S. Shimizu, J. Hirota, T. Takao, Y. Fan, Y. Matsuoka, L. Zhang, Y. Yoneda, Y. Fujii, A. I. Skoultchi, Y. Tsujimoto, Involvement of histone H1.2 in apoptosis induced by DNA double-strand breaks. *Cell* **114**, 673–688 (2003). doi:10.1016/S0092-8674(03)00719-0 Medline

10. A. Jhingran, K. B. Mar, D. K. Kumasaka, S. E. Knoblaugh, L. Y. Ngo, B. H. Segal, Y. Iwakura, C. A. Lowell, J. A. Hamerman, X. Lin, T. M. Hohl, Tracing conidial fate and measuring host cell antifungal activity using a reporter of microbial viability in the lung. *Cell Reports* **2**, 1762–1773 (2012). doi:10.1016/j.celrep.2012.10.026 Medline

11. G. Ambrosini, C. Adida, D. C. Altieri, A novel anti-apoptosis gene, *survivin*, expressed in cancer and lymphoma. *Nat*. *Med*. **3**, 917–921 (1997). doi:10.1038/nm0897-917 Medline

12. F. Li, P. L. Flanary, D. C. Altieri, H. G. Dohlman, Cell division regulation by BIR1, a member of the inhibitor of apoptosis family in yeast. *J*. *Biol*. *Chem*. **275**, 6707–6711 (2000). doi:10.1074/jbc.275.10.6707 Medline

13. Q. L. Deveraux, J. C. Reed, IAP family proteins: Suppressors of apoptosis. *Genes Dev*. **13**, 239–252 (1999). doi:10.1101/gad.13.3.239 Medline

14. S. Shin, B. J. Sung, Y. S. Cho, H. J. Kim, N. C. Ha, J. I. Hwang, C. W. Chung, Y. K. Jung, B. H. Oh, An anti-apoptotic protein human survivin is a direct inhibitor of caspase-3 and -7. *Biochemistry* **40**, 1117–1123 (2001). doi:10.1021/bi001603q Medline

15. A. Berezov, Z. Cai, J. A. Freudenberg, H. Zhang, X. Cheng, T. Thompson, R. Murali, M. I. Greene, Q. Wang, Disabling the mitotic spindle and tumor growth by targeting a cavity-induced allosteric site of survivin. *Oncogene* **31**, 1938–1948 (2012). doi:10.1038/onc.2011.377 Medline

16. T. M. Hohl, A. Rivera, L. Lipuma, A. Gallegos, C. Shi, M. Mack, E. G. Pamer, Inflammatory monocytes facilitate adaptive CD4 T cell responses during respiratory fungal infection. *Cell Host Microbe* **6**, 470–481 (2009). doi:10.1016/j.chom.2009.10.007 Medline

17. S. M. Holland, Chronic granulomatous disease. *Clin*. *Rev*. *Allergy Immunol*. **38**, 3–10 (2010). doi:10.1007/s12016-009-8136-z Medline

18. A. Casadevall, L. Pirofski, Host-pathogen interactions: The attributes of virulence. *J*. *Infect*. *Dis*. **184**, 337–344 (2001). doi:10.1086/322044 Medline

19. A. Sharon, A. Finkelstein, N. Shlezinger, I. Hatam, Fungal apoptosis: Function, genes and gene function. *FEMS Microbiol*. *Rev*. **33**, 833–854 (2009). doi:10.1111/j.1574-6976.2009.00180.x Medline

20. N. Shlezinger, A. Doron, A. Sharon, Apoptosis-like programmed cell death in the grey mould fungus *Botrytis cinerea*: Genes and their role in pathogenicity. *Biochem*. *Soc*. *Trans*. **39**, 1493–1498 (2011). doi:10.1042/BST0391493 Medline

21. K. Z. Hein, H. Takahashi, T. Tsumori, Y. Yasui, Y. Nanjoh, T. Toga, Z. Wu, J. Grötzinger, S. Jung, J. Wehkamp, B. O. Schroeder, J. M. Schroeder, E. Morita, Disulphide-reduced psoriasin is a human apoptosis-inducing broad-spectrum fungicide. *Proc*. *Natl*. *Acad*. *Sci*. *U*.*S*.*A*. **112**, 13039–13044 (2015). doi:10.1073/pnas.1511197112 Medline

22. K. Shimizu, N. P. Keller, Genetic involvement of a cAMP-dependent protein kinase in a G protein signaling pathway regulating morphological and chemical transitions in *Aspergillus nidulans*. *Genetics* **157**, 591–600 (2001). Medline

23. M. M. Mircescu, L. Lipuma, N. van Rooijen, E. G. Pamer, T. M. Hohl, Essential role for neutrophils but not alveolar macrophages at early time points following *Aspergillus fumigatus* infection. *J*. *Infect*. *Dis*. **200**, 647–656 (2009). doi:10.1086/600380 Medline

24. Ö. Bayram, O. S. Bayram, Y. L. Ahmed, J. Maruyama, O. Valerius, S. O. Rizzoli, R. Ficner, S. Irniger, G. H. Braus, The *Aspergillus nidulans* MAPK module AnSte11-Ste50-Ste7-Fus3 controls development and secondary metabolism. *PLOS Genet*. **8**, e1002816 (2012). doi:10.1371/journal.pgen.1002816 Medline

25. M. M. Yelton, J. E. Hamer, W. E. Timberlake, Transformation of *Aspergillus nidulans* by using a trpC plasmid. *Proc*. *Natl*. *Acad*. *Sci*. *U*.*S*.*A*. **81**, 1470–1474 (1984). doi:10.1073/pnas.81.5.1470 Medline

26. S. W. Biel, F. W. Parrish, Isolation of DNA from fungal mycelia and sclerotia without use of density gradient ultracentrifugation. *Anal*. *Biochem*. **154**, 21–25 (1986). doi:10.1016/0003-2697(86)90489-6 Medline

27. C. P. Semighini, S. D. Harris, Methods to detect apoptotic-like cell death in filamentous fungi. *Methods Mol. Biol.* **638**, 269–279 (2010). doi:10.1007/978-1-60761-611-5_20 Medline

28. S. Barhoom, A. Sharon, Bcl-2 proteins link programmed cell death with growth and morphogenetic adaptations in the fungal plant pathogen *Colletotrichum gloeosporioides*. *Fungal Genet. Biol.* **44**, 32–43 (2007). doi:10.1016/j.fgb.2006.06.007 Medline

29. T. M. Hohl, H. L. Van Epps, A. Rivera, L. A. Morgan, P. L. Chen, M. Feldmesser, E. G. Pamer, *Aspergillus fumigatus* triggers inflammatory responses by stage-specific beta-glucan display. *PLOS Pathog.* **1**, e30 (2005). doi:10.1371/journal.ppat.0010030 Medline

30. E. Szewczyk, S. Krappmann, Conserved regulators of mating are essential for *Aspergillus fumigatus* cleistothecium formation. *Eukaryot. Cell* **9**, 774–783 (2010). doi:10.1128/EC.00375-09 Medline

31. E. Szewczyk, T. Nayak, C. E. Oakley, H. Edgerton, Y. Xiong, N. Taheri-Talesh, S. A. Osmani, B. R. Oakley, Fusion PCR and gene targeting in *Aspergillus nidulans*. *Nat. Protoc.* **1**, 3111–3120 (2007). doi:10.1038/nprot.2006.405 Medline

32. A. Sasse, S. N. Hamer, J. Amich, J. Binder, S. Krappmann, Mutant characterization and in vivo conditional repression identify aromatic amino acid biosynthesis to be essential for *Aspergillus fumigatus* virulence. *Virulence* **7**, 56–62 (2016). doi:10.1080/21505594.2015.1109766 Medline

33. F. N. Gravelat, D. S. Askew, D. C. Sheppard, Targeted gene deletion in *Aspergillus fumigatus* using the hygromycin-resistance split-marker approach. *Methods Mol. Biol.* **845**, 119–130 (2012). doi:10.1007/978-1-61779-539-8_8 Medline